ACS OMEGA

Open Access

http://pubs.acs.org/journal/acsodf

Article

Molecular Dynamics Simulation on the Suppression Mechanism of Phosphorylation to Ser222 by Allosteric Inhibitors Targeting MEK1/2 Kinase

Sathish K. Mudedla, Hayoung Lee, Jeom Ji Kim, Seong Hun Jang, Munikumar R. Doddareddy, Swetha Y. Sanam, Rochish Gundabathula, Jang-June Park, and Sangwook Wu*

Cite This: *ACS Omega* 2024, 9, 31946−31956

Read Online

ACCESS | Metrics & More | Article Recommendations | Supporting Information

ABSTRACT: Allosteric inhibitors of mitogen-activated protein kinase 1 (MEK1) reveal distinct interactions with MEK1 activation loop residues. The structural analyses will determine whether, and how, distinct inhibitors suppress the phosphorylation of MEK1 and may guide future therapeutic development. In this study, we explored the suppression mechanism of the phosphorylation process in the presence of MEK allosteric inhibitors, such as selumetinib, trametinib, cobimetinib, and CH5126766, by employing molecular dynamics simulations accompanied by principal component analysis. The simulations of wildtype MEK1 show that Ser222 can come close to γ-phosphate but not Ser218. We have found the conformation where Ser222 is within 5 Å of distance, which makes Ser222 accessible for γ-phosphate. The conformation analysis from the simulations of MEK1 in the presence of allosteric inhibitors reveals that the inhibitor restricts the flexibility of Ser222 through strong interactions with the activation loop, Lys97, and water mediates interactions with amino acids in the vicinity. The results reveal that all the inhibitors act as screeners between the activation loop and Mg-ATP and restricting the flexibility of the activation loop through strong interaction causes the suppression of the phosphorylation process of MEK1. The results conclude that a strong interaction of allosteric inhibitors with the activation loop restricts the movement of Ser222 toward Mg-ATP, which could be the dominant factor for the suppression of phosphorylation in MEK1. This research will provide novel insights to design effective anticancer therapeutics for targeting MEK1 in the future.

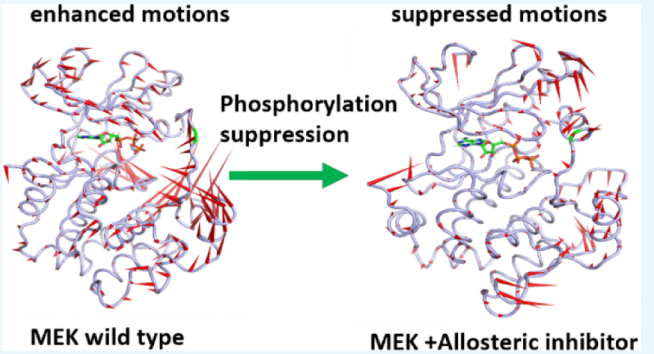

INTRODUCTION

Extracellular signal-regulated kinase 1/2 is a member of the mitogen-activated protein kinase (MAPK) family.[1] Its primary function involves participating in signaling cascades that facilitate the transmission of extracellular signals to intracellular targets. Consequently, MAPK cascades represent pivotal components of the signaling pathway, governing fundamental cellular processes like cell proliferation, differentiation, and stress responses.[1−3] Dysfunction of this pathway has been associated with several diseases such as inflammation, chronic obstructive pulmonary disease, influenza, cardio-fascio-cutaneous syndrome, and neuropathic pain.[4−7] In particular, considerable resources have been committed to the search for novel inhibitors targeting the extracellular signal regulated kinase (ERK) pathway, with a particular focus on one of its components, MEK1 and MEK2. These proteins exhibit broad cellular expression and play integral roles within the signal transduction cascade known as the MAPK cascade.[8,9]

MEK1 and MEK2 serve as dual-specificity protein kinases, facilitating phosphorylation on both tyrosine and threonine residues to activate ERK1 and ERK2. These kinases are themselves phosphorylated and activated by RAF kinases and exhibit relatively restricted substrate specificity. The initial discovery in the realm of ERK pathway inhibition, PD98059, was documented as the first of its kind and demonstrated its mechanism of action as an apparent allosteric inhibitor for MEK1 and MEK2, operating independently of ATP.[10] Subsequently, MEK inhibitors (MEKis) have established themselves as indispensable research instruments, essential for expanding our understanding of ERK1 and ERK2 biology, while also affirming the significance of MEK1 and MEK2 as potential targets for cancer therapy.[11,12]

Human MEK1 comprises an N-terminal segment, a protein kinase domain, and a C-terminal region.[13] Within the N-

Received: April 15, 2024
Revised: June 18, 2024
Accepted: June 20, 2024
Published: July 10, 2024

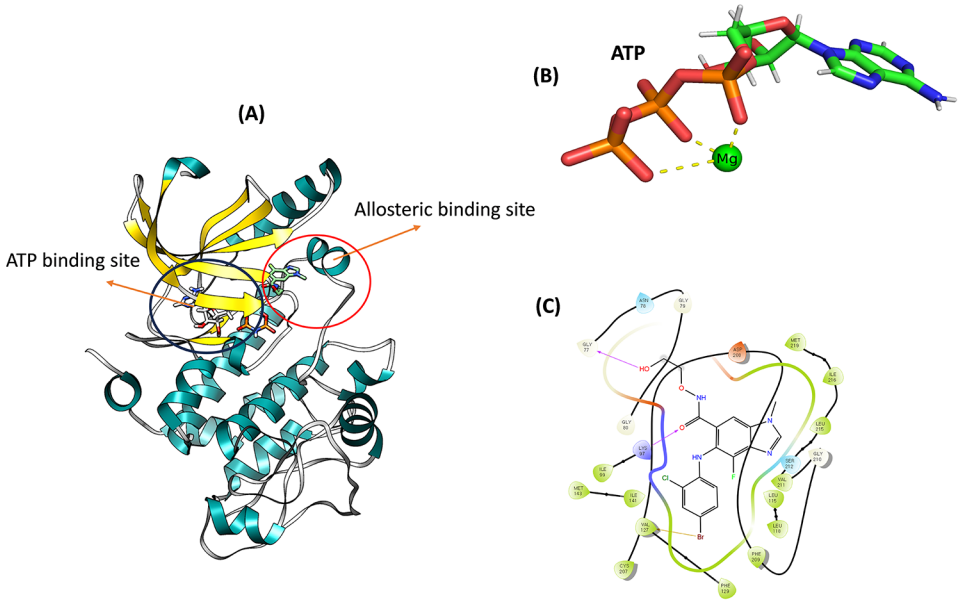

Figure 1. Overall structure of MEK1 with ATP and the allosteric inhibitor, selumetinib. Carbon atom of ATP is colored white, and that of selumetinib is colored green. Secondary structure of the protein is colored differently, helix as dark cyan, beta-strand as gold, and coil as gray. (A) MEK structure with ATP and allosteric inhibitors. (B) Mg-ATP. (C) 2D interaction diagram of allosteric inhibitor.

terminus, there is an inhibitory segment (residues 43−59) that plays a role in the interaction between MEK1 and its ERK substrates. The N-terminal lobe of MEK1 contains the conserved glycine-rich ATP-phosphate-binding loop (P-loop), and the active site of MEK1 is facilitated by eight specific residues, aiding in the binding of both ATP and competitive inhibitors.[14]

MEK1 exists in different conformations, and its activity is regulated through phosphorylation and dephosphorylation processes.[15] The key amino acids involved in these processes are typically serine (S) and threonine (T) residues. Phosphorylation of MEK1 at specific serine and threonine residues activates its kinase activity. In the case of MEK1, these phosphorylation sites are Ser218 and Ser222. Phosphorylation of these serine residues leads to a conformational change in MEK1, exposing its active site, which can then phosphorylate ERK (extracellular signal-regulated kinase).[16,17] The phosphorylation of MEK1 is often catalyzed by upstream kinases, such as RAF kinases.[18] Dephosphorylation of MEK1 at Ser218 and Ser222 occurred through the action of protein phosphatases, such as protein phosphatase 2A (PP2A), resulting in the inactivation of MEK1.[19,20] MEK1 in its dephosphorylated state has lower kinase activity and cannot activate downstream targets like ERK. The low- and high-activity states can adopt different conformations that demonstrate various interactions with ligands and inhibitors. Substituting serine residues in the activation segment with negatively charged residues, such as glutamate or aspartate, partially mimics phosphorylation and results in a constitutively activated kinase.[21−25]

Investigations into the crystal structures of MEK1/2 have unveiled two distinct binding pockets: the orthosteric and allosteric inhibitors.[26] The orthosteric pocket accommodates ATP and ATP-analogues, while allosteric inhibitors find their binding sites in the allosteric pocket. A significant feature of this arrangement is the physical separation between the allosteric inhibitor binding pocket and the Mg-ATP binding pocket, shielded by the strategically positioned side chains of Lys97 and Met143, which remain conserved in the MEK active site.[27,28] The engagement of allosteric inhibitors in this binding pocket initiates a vital hydrogen-bond interaction and establishes numerous noncovalent connections within the hydrophobic pocket, which is defined by a cluster of residues. This interaction induces a series of conformational alterations within MEK, ultimately resulting in the perturbation of the catalytic residue Lys97 and the consequent inactivation of MEK's enzymatic activity.

In the quest to modulate MEK1, researchers have crafted a variety of allosteric inhibitors that precisely target this allosteric pocket.[29−32] The allosteric inhibitors are renowned for establishing robust hydrogen bond interactions with Ser212. This interaction effectively constrains the activation loop, impeding subsequent phosphorylation by RAF. The ability to disrupt MEK1/2 phosphorylation is closely associated with the extent to which an inhibitor coordinates with Asn221 and Ser222, subsequently displacing the activation loop. For instance, CH5126766 adeptly binds both Asn221 and Ser222, inducing activation loop displacement.[33] Conversely, an enantiomer nearly identical to PD0325901 fails to coordinate Asn221 and Ser222 or displace the activation loop, reflecting their varying efficacy in disrupting MEK1 and MEK2 phosphorylation.[34] The question of whether these inhibitors can effectively antagonize phosphorylation at both Ser218 and Ser222 of MEK1, as well as Ser222 and Ser226 of MEK2, remains a subject of exploration. Hence, in this study, we explored the suppression mechanism of the phosphorylation process in the presence of MEK allosteric inhibitors such as selumetinib, trametinib, cobimetinib, pimasertib, and CH5126766 by employing classical molecular dynamics simulations and essential dynamics analysis.

Computational Details. The crystal structure of MEK1 was downloaded from the protein databank (PDB id: 4u7z).[35] The ATP and magnesium ions were introduced to the MEK1 structure with the aid of other crystal structures. The missing residues from 270 to 306 were built using the MEK structure from the Alpha fold2.[36,37] The allosteric and ATP binding sites are listed in Figure 1.

https://doi.org/10.1021/acsomega.4c03615
ACS Omega 2024, 9, 31946−31956

The chemical structures of all of the considered inhibitors are shown in Figure 2.

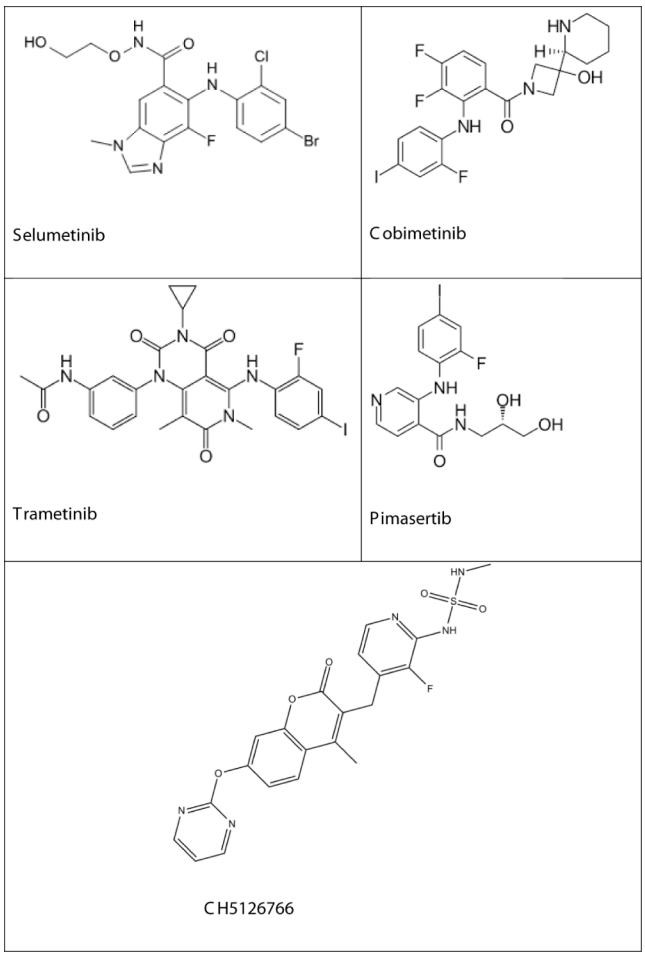

Figure 2. Two-dimensional structures of allosteric inhibitors considered in this study.

The inhibitors were docked at the allosteric site using Autodock Vina.[38,39] The alignment of the docked ligand molecule is correlated to the inhibitor in the crystal structure. MD simulations were performed for the complex of MEK and inhibitors with Mg-ATP using the GROMACS-2020 package.[40−42] AMBER99SB-ildn force field parameters were used for the protein. The Lennard-Jones parameters for Mg were taken from the literature.[43,44] The structures of selumetinib, trametinib, cobimetinib, and CH5126766 were optimized using density functional theory (DFT) calculations by employing the Gaussian16 package using the B3LYP/6-31G** level of theory.[45] The charges and force field parameters were generated for inhibitors using the antechamber program.[46] The complex was solvated in a cubic box with a TIP3P water model.[47] The total charge of the complex was neutralized by adding 0.15 nM of NaCl. The solvated structures were energy-minimized using the steepest decent algorithm.[48] The minimized structures were carried out for equilibration at 298 K and 1 bar pressure for 1 ns by imposing positional restraints on the structures. Velocity rescaling and Parrinello Rahman algorithms were applied to control the temperature and pressure.[49,50] The electrostatic interactions were calculated using the particle mesh Ewald method,[51] and bonds between hydrogen and heavy atoms were constrained with the help of the LINCS algorithm.[52] The production run was performed for 100 ns in the NPT ensemble. The structures were visualized and analyzed using Pymol.[53] Root-mean-square deviation (RMSD) and radius of gyration were calculated for MEK1 by excluding the highly flexible loop region (residues from 270 to 306) for all of the cases.

To evaluate the binding free energies of protein and ligand complexes, we employed the free energy perturbation (FEP)[54,55] method within an explicit water environment. Starting with the final snapshot from 100 ns molecular dynamics simulations, this method involved a two-step process. First, we decoupled the ligand from the protein−ligand complex in an explicit water environment, and second, we decoupled the ligand from the water environment. The intricate decoupling process entailed gradually deactivating van der Waals and electrostatic interactions responsible for complex formation (protein−ligand or water−ligand) using the coupling parameter (λ). Initially, electrostatic interactions were systematically turned off, while van der Waals interactions persisted. Subsequently, we ceased van der Waals interactions between the protein and ligand (water and ligand) using the coupling parameter (λ). The deactivation of electrostatic interactions involved a stepwise change in λ (0, 0.25, 0.5, 0.75, and 1.0) from 0 to 1 with a step size of $\Delta\lambda$ = 0.25. van der Waals interactions were turned off with nonuniformly distributed values of λ (0.05, 0.1, 0.2, 0.3, 0.4, 0.5, 0.6, 0.65, 0.7, 0.75, 0.8, 0.85, 0.9, 0.95, and 1.0). This procedure was applied to decouple ligands from both the protein−ligand complex and the water environment. Consequently, we employed 21 windows, each spanning 1 ns, to systematically untether the ligand from the protein−ligand and water−ligand complexes. To compute the free energy difference between the two end states, we utilized the Bennett acceptance ratio (BAR) method.[56] The BAR method is used to estimate the free energy difference between two states with the following equation:

$$\left\langle \frac{1}{1+\exp\{\beta(\Delta U_{ij}-\Delta G)\}} \right\rangle i = \left\langle \frac{1}{1+\exp\{\beta(-\Delta U_{ij}+\Delta G)\}} \right\rangle j \quad (1)$$

where β is the reciprocal of the thermodynamic temperature, ΔG is the free energy difference between states i and j, and $\Delta U_{ij} = U_j - U_i$ is the potential energy difference.

For every λ-point, we performed energy minimization on the structures using the steepest descent method. Subsequently, employing Langevin dynamics, we subjected the resulting structures to equilibration within an isothermal−isobaric (NPT) ensemble, maintaining conditions at 298 K and 1 bar of pressure. The remainder of the simulation protocol closely mirrored the procedures outlined in the classic molecular dynamics (MD) section.

RESULTS AND DISCUSSION

Figure 3 shows that the RMSD of backbone of MEK1 in the case of apo and complexes with inhibitors reaches acceptable equilibrium after 20 ns of simulations. We have carried out three independent simulations for all the complexes, and the resulted trajectories did not show any significant differences between them. The calculated RMSD for three independent simulations is shown in Figure S1. Mg-ATP is stable at the

https://doi.org/10.1021/acsomega.4c03615
ACS Omega 2024, 9, 31946−31956

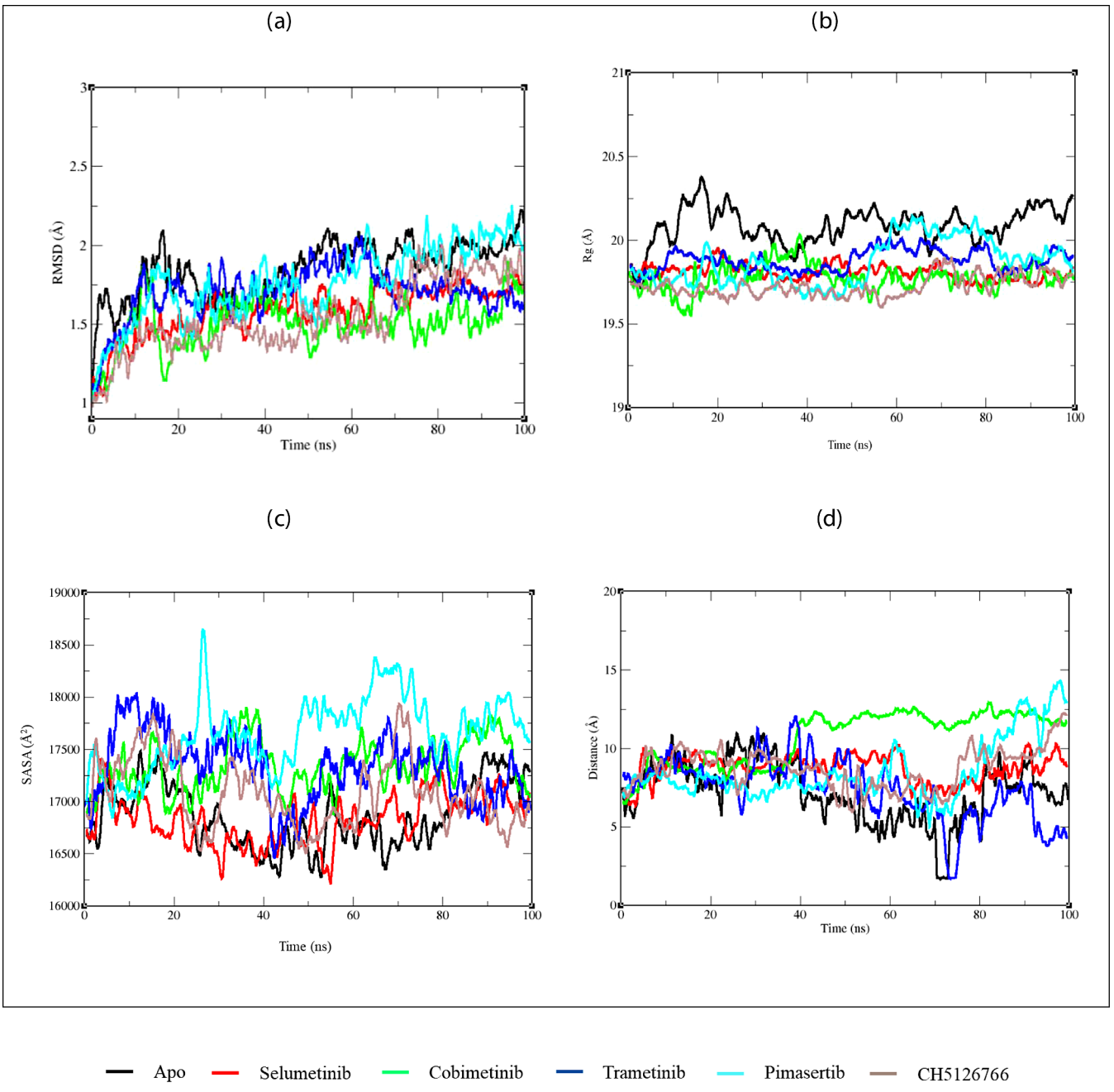

Figure 3. (a) Root-mean-square deviation, (b) radius of gyration, (c) solvent accessible surface area, and (d) distance between Ser222 and ATP. Running averages have been taken for clear visualization. Each allosteric inhibitor is denoted by a color.

orthosteric site throughout the simulation of MEK-Mg-ATP. The coordination around the Mg ion is not disturbed during the simulation. The RMSD values range from 1 to 2.25 Å. The RMSD values are slightly higher for apo MEK than for the complexes of inhibitors. All of the inhibitors stabilize MEK more than the apo state. The calculated radius of gyration (Rg) helps us to understand the overall shape and size variations of MEK in the presence of allosteric inhibitors and ATP. Rg shows the conformational changes in MEK in the presence of inhibitors. The average variations in MEK presented by Rg of apo, selumetinib, cobimetinib, trametinib, pimasertib, and CH5126766 are 20.0, 19.8, 19.7, 19.8, 19.8, and 19.7 Å, respectively. It is clear from Figure 3 that apo MEK has a higher Rg value than the allosteric inhibitors. The lowest Rg is found for cobimetinib and CH5126766. A large value of Rg corresponds to the wide conformational distribution of MEK1 in the apo state. The lower value for cobimetinib and CH5126766 suggests the higher compactness of MEK1. It is clear that the compactness of the protein increases after binding with allosteric inhibitors. Each inhibitor exhibits different Rg values due to variations in its chemical structures. The surface area of MEK1 that is accessible to the solvent is shown in Figure 3. It shows that the solvent-accessible surface area (SASA) is increased for apo and pimasertib, whereas the same is decreased in the case of selumetinib. However, no clear pattern is observed for cobimetinib, trametinib, and CH5126766. Their SASA values fluctuate between 160.0 and 175.0 nm.[2] The average SASA of MEK1 is 171.0, 164.8, 169.4,

https://doi.org/10.1021/acsomega.4c03615
ACS Omega 2024, 9, 31946−31956

168.2, 173.3, and 166.9 nm^2 for apo, selumetinib, cobimetinib, trametinib, pimasertib, and CH5126766, respectively. These results indicate that MEK1 expanded in the case of apo. A possibility may be due to the local unfolding of secondary structures. The loss of secondary structure may lead to less stability of MEK1, whereas selumetinib increases the stability of MEK1 by retaining the local folded conformations. The variations in RMSD, Rg, and SASA of MEK1 occurred due to the flexible activation loop region. The minimum distance between Ser222 and the ATP molecule was analyzed to understand the flexibility of the activation loop. In the starting conformation, the distance between Ser222 is around 14 Å from the γ-phosphate of ATP. The calculated distance between Ser222 and γ- phosphate in Figures 3 and S2 shows the wide range of distance distribution in apo, selumetinib, cobimetinib, trametinib, pimasertib, and CH5126766. The activation loop moves toward and away from ATP. The predominant structures of MEK1 have an activation loop moved away from ATP in the case of apo and allosteric inhibitors. However, it is noted that an ensemble of conformations is in close contact with ATP within 2 Å in the case of apo and trametinib. The distance distribution is wide in the case of apo compared to that of allosteric inhibitors. These structures make Ser222 accessible for γ-phosphate to initiate the phosphorylation process. Allosteric inhibitors do not allow the movement of Ser222 in the activation loop toward ATP leading to the suppression of the phosphorylation process in the presence of considered inhibitors.

Interactions of Allosteric Inhibitors with MEK1. All of the allosteric inhibitors have crucial interactions with Ser212, Phe209, Val127, and Lys97. Ser212 and Phe209 are away from the activation loop. Lys97 is important for its catalytic activity. The two-dimensional interaction diagrams of allosteric inhibitors are shown in Figure 4. Selumetinib, cobimetinib, trametinib, and pimasertib have interactions with the activation loop and Lys97, whereas CH5126766 does not interact with Lys97. It can be noted that a few of the inhibitors have additional interactions other than the activation loop and Lys97.

The shapes of the considered allosteric inhibitors differ from each other. The binding affinity and specificity of the inhibitor determine the strength of the interaction with MEK1. Due to variations in the shape of the molecule, the resulting structural changes in MEK1 are varied with each inhibitor, which can be seen from Rg and SASA analysis. The activity of the inhibitor depends on how strongly it can hold the activation loop and Lys97 to prevent their participation in the phosphorylation process. Hence, the interaction between ATP and Lys97 is calculated throughout the simulation of each inhibitor and shown in Figure 5.

Selumetinib, cobimetinib, trametinib, and pimasertib prevent the participation of Lys97 in the phosphorylation process by increasing the distance between Lys97 and ATP. The distance ranges from 3 to 4 Å. On the other hand, the same distance lies within 2−3 Å in the case of apo and CH5126766. ATP has hydrogen bond interactions with Lys97 for apo and CH5126766, which can facilitate the phosphorylation process through the involvement of Lys97. The absence of interaction between Lys97 and CH5126766 may reduce its ability to suppress the phosphorylation process. This result is in agreement with the previous experimental report,[33] where they have shown the reduced activity for CH5126766 for isolated MEK1, and it may be because of the lack of Lys97 interaction. Another experimental study has presented the importance of Lys97 in the phosphorylation process, and mutation of Lys97 leads to suppression of autophosphorylation.[57] The increased distance between Lys97 and ATP in the presence of inhibitors (selumetinib, cobimetinib, trametinib, and pimasertib) is due to their strong interaction with Lys97. Selumetinib, pimasertib, and trametinib interact with Lys97 through the carbonyl group, but it is the halogen atom for cobimetinib. The estimated distance between Lys97 and inhibitors is shown in Figure 5. In addition, Ser212, Phe209, and Val127 interactions are also stable throughout the MD simulations for all of the inhibitors during 100 ns. We have noticed that a few pharmacophore characteristics of allosteric inhibitors are (i) distance between Lys97 and Ser212, (ii) angle between Lys97, inhibitors, and Ser212, and (iii) triangle formation between Lys97, Val127, and Ser212.

Figure 6 shows the distance between Lys97 and Ser212 in the case of apo and inhibitors. The distance decreases for apo as the activation loop is free to fluctuate toward Lys97. The movement causes flexibility in Ser222 and Ser212. The same distance is stable at around 10 Å for allosteric inhibitors, except in the case of pimasertib. The decrease in the distance for

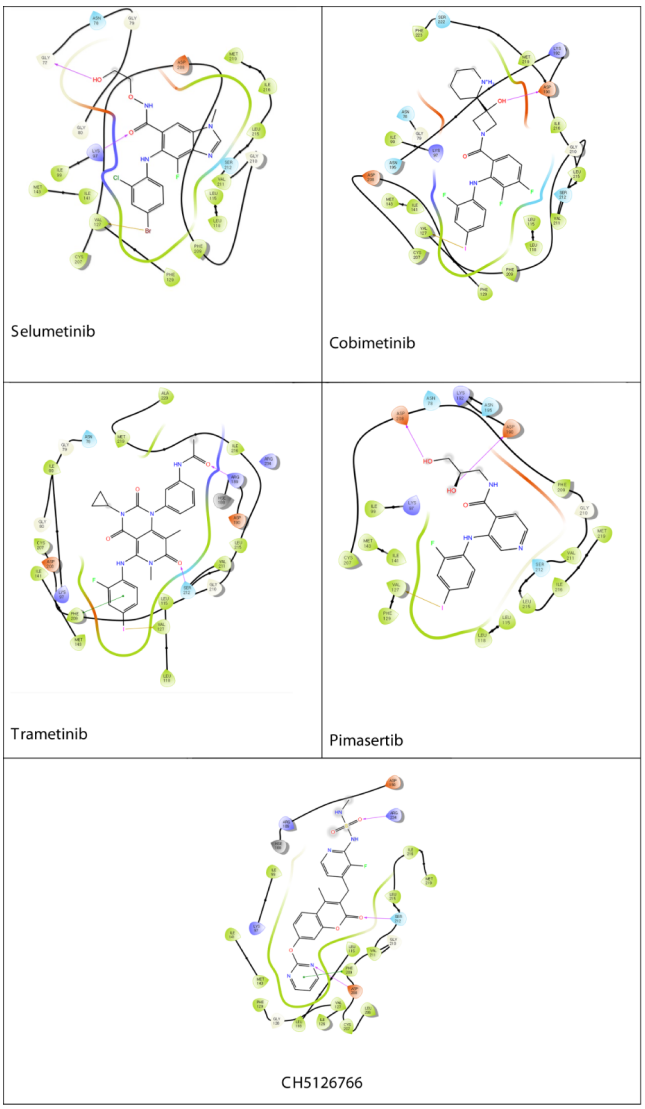

Figure 4. Two-dimensional interaction diagrams for allosteric inhibitors with MEK1.

https://doi.org/10.1021/acsomega.4c03615
ACS Omega 2024, 9, 31946−31956

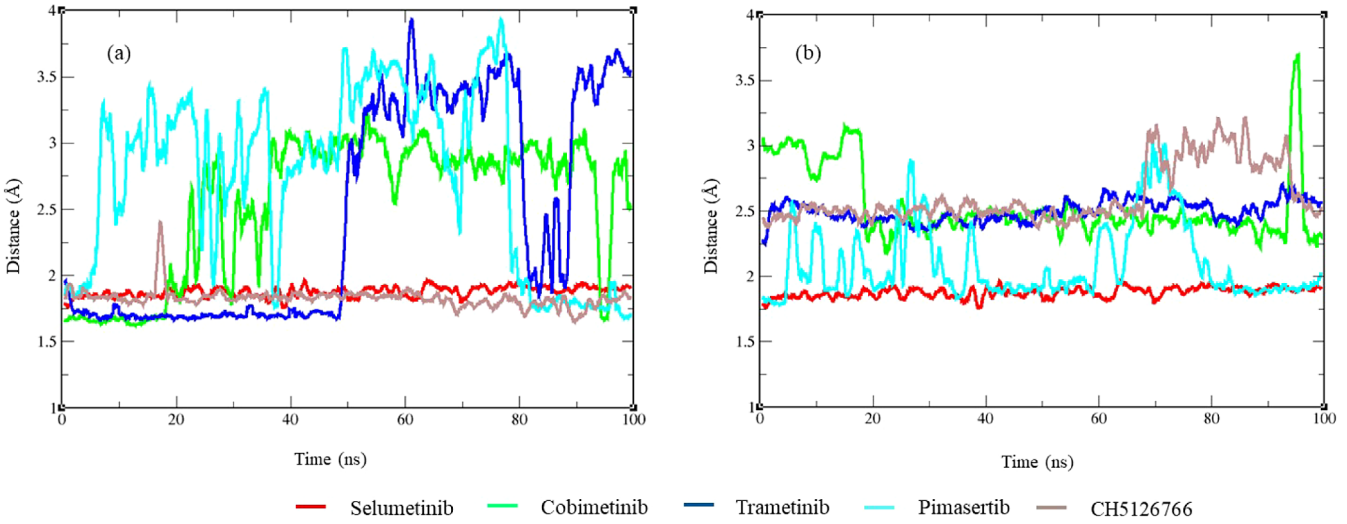

Figure 5. (A). Distance between ATP and Lys97. (B) Distance between Lys97 and the inhibitor. Running averages have been taken for all the distances for clear visualization. The distance of each allosteric inhibitor is denoted by a color.

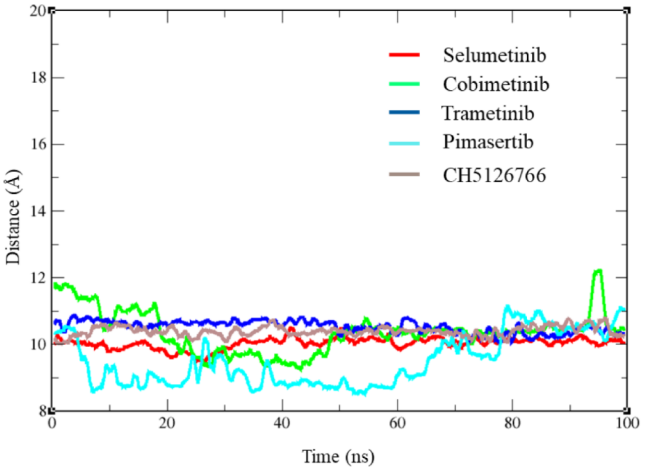

Figure 6. Minimum distance between Ser212 and Lys97. Running averages have been taken for all the distances for clear visualization. The distance of each allosteric inhibitor is denoted by a color.

pimasertib is due to the available space between Lys97 and Ser212. In all the inhibitors, the space occupied by the presence of fused rings interacts with Ser212, whereas pimasertib has a single aromatic ring that does not fit exactly between Lys97 and Ser212. The unoccupied space allows movement of the activation loop, which might also affect the flexibility of Ser222. It is important for the suppression of the phosphorylation process. The angle used to measure the planarity in the interaction between Lys97, Ser212, and inhibitors, as well as the triangle formation within the allosteric site is defined in Figure 7.

From Figure 8, the estimated angles of Lys97, inhibitors, and Ser212 show that they are planar in selumetinib, cobimetinib, trametinib, and pimasertib. The angle between the interacting atoms with Ser212, Lys97, and Val127 forms a triangle in all the inhibitors, and the results are shown in Figure 9. The results reveal that characteristics such as distance between Lys97 and Ser212, planarity, and triangle formation are subtle properties of allosteric inhibitors to restrict the flexibility of the activation loop and catalytic Lys97 to suppress the phosphorylation process.

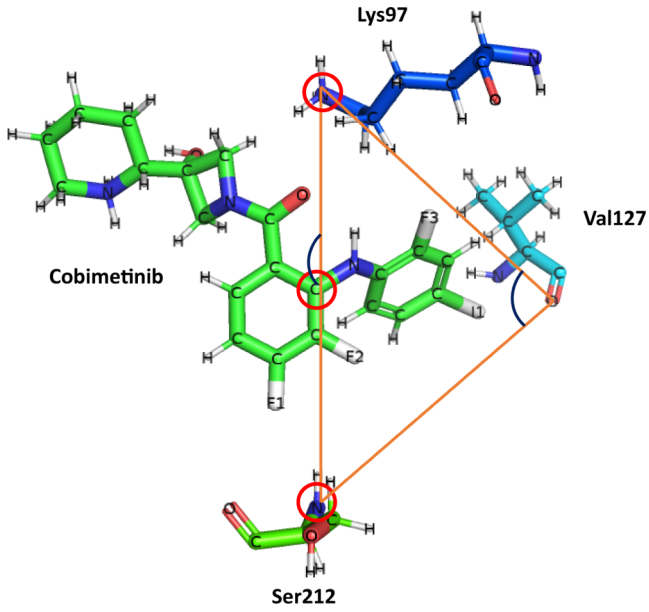

Figure 7. Definition of the planar angle and triangle formation. Planar angle forms between Lys97, inhibitors (carbon atom in the circle), and Ser212. Triangle forms between Lys97, Ser212, and Val127.

Free Energy Calculations. Additionally, a comparative analysis was conducted by juxtaposing the computed alchemical free energies with the corresponding experimental IC_{50} values for a designated set of MEK1 inhibitors, as delineated in Table 1. The results presented reveal a discernible correlation between these two data sets, affirming the fidelity of our alchemical free energy calculations in accurately encapsulating the thermodynamic intricacies of ligand binding. Specifically, trametinib, cobimetinib, and selumetinib, with IC_{50} values below 15 nM, exhibit free energy values within the range of approximately −20 kcal/mol and above. Notably, the experimental IC_{50} value of pimasertib, correlated with cell lines, has been singularly assessed without direct comparison to those of other ligands. Nevertheless, its calculated free energy value of −16.95 kcal/mol underscores its robust binding affinity to MEK1.

https://doi.org/10.1021/acsomega.4c03615
ACS Omega 2024, 9, 31946−31956

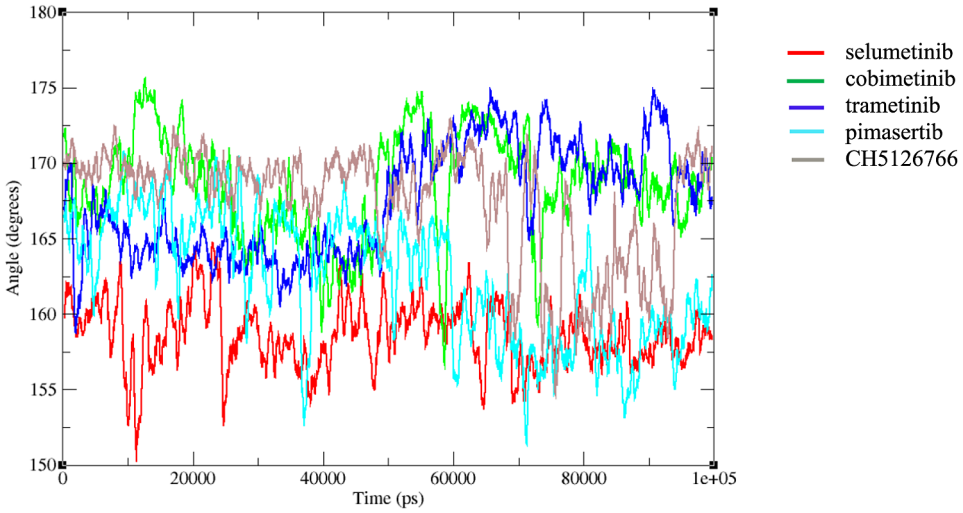

Figure 8. Calculated angle between Lys97, inhibitors, and Ser212. This angle is used to measure the planarity in the interaction between Lys97, inhibitors, and Ser212. Running averages have been taken for all the angles for clear visualization. The angles for each allosteric inhibitor are denoted by a different color.

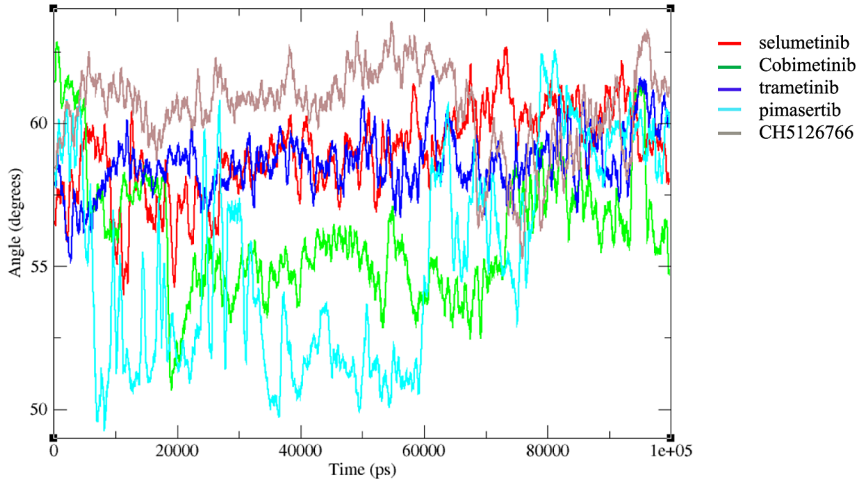

Figure 9. Calculated angle between Lys97, Ser212, and Val127. This angle is used to measure the triangle formation while interaction with inhibitors. Running averages have been taken for all the angles for clear visualization. The angles for each allosteric inhibitor are denoted by a different color.

Table 1. Calculated Free Energies of MEK1 Inhibitors and Their Experimental IC_{50} Values

inhibitor	IC_{50}	free energy (kcal/mol)
trametinib	0.92 nM	−24.55 ± 0.53
cobimetinib	4.2 nM	−19.58 ± 1.16
pimasertib	5 nM−2 μM (cell activity)	−16.95 ± 0.97
selumetinib	14 nM	−22.85 ± 0.77

Intriguingly, a deviation was observed in the free energy value of CH5126766 (not shown in Table 1). The incongruity between the calculation and IC_{50} value could be attributed to the inherent limitations of free energy methods when applied to large and flexible ligands, such as CH5126766, which surpasses the others in size. The complexities associated with the conformational flexibility and size of CH5126766 may impede the accuracy of the free energy predictions, thereby elucidating the observed disparity from the experimental trend.

Secondary Structural Changes in the Activation Segment. The activation loop (Ile216 to Ser222) forms a small helix. The previous studies show that the secondary structure conformation plays a role in activating MEK1 by phosphorylation and activated mutants.[58] The active mutations and phosphorylation can cause the helix conformation to disappear, whereas the nonactive conformation retains 90% of the helical content in the activation loop. The active mutations reduced helical content of the activation loop to less than 10%.[58] Hence, the estimated average helical content of the activation loop with seven residues throughout the 100 ns simulation for apo, selumetinib, cobimetinib, trametinib, pimasertib, and CH5126766 is 0%, 10%, 27%, 1%, 9%, and 21%, respectively. It can be noted that helical content is significantly decreased and is switched to the loop in the case of apo with ATP. The small helix of the activation loop is transformed to the loop conformation in the case of wild type and trametinib. The other allosteric inhibitors hold the helical conformation of the activation loop, and the retention of helical content is more than 20% in the case of cobimetinib and CH5126766. The allosteric inhibitors restrict the

https://doi.org/10.1021/acsomega.4c03615
ACS Omega 2024, 9, 31946−31956

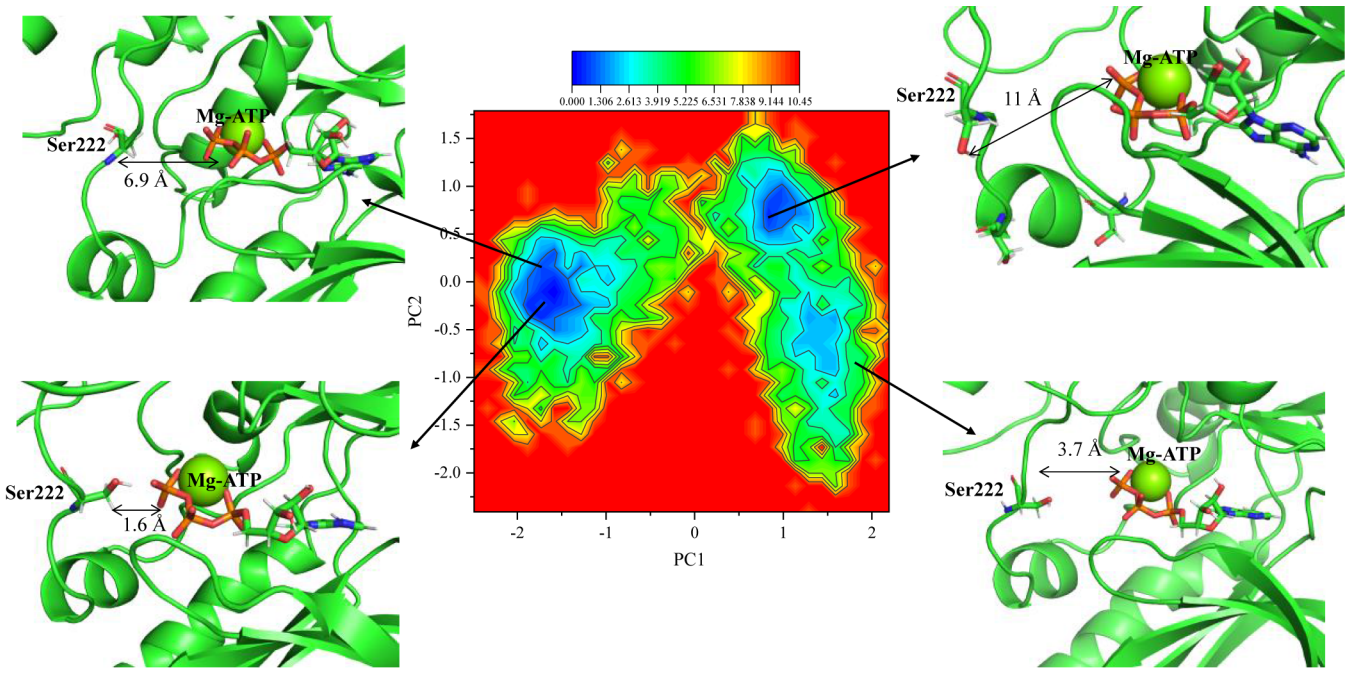

Figure 10. Free energy landscape of MEK1 with ATP. Free energy landscape is derived by using the projection of principal component-1 (PC1) and principal component-2 (PC2). Blue color represents low-energy regions, and red indicates high-energy regions.

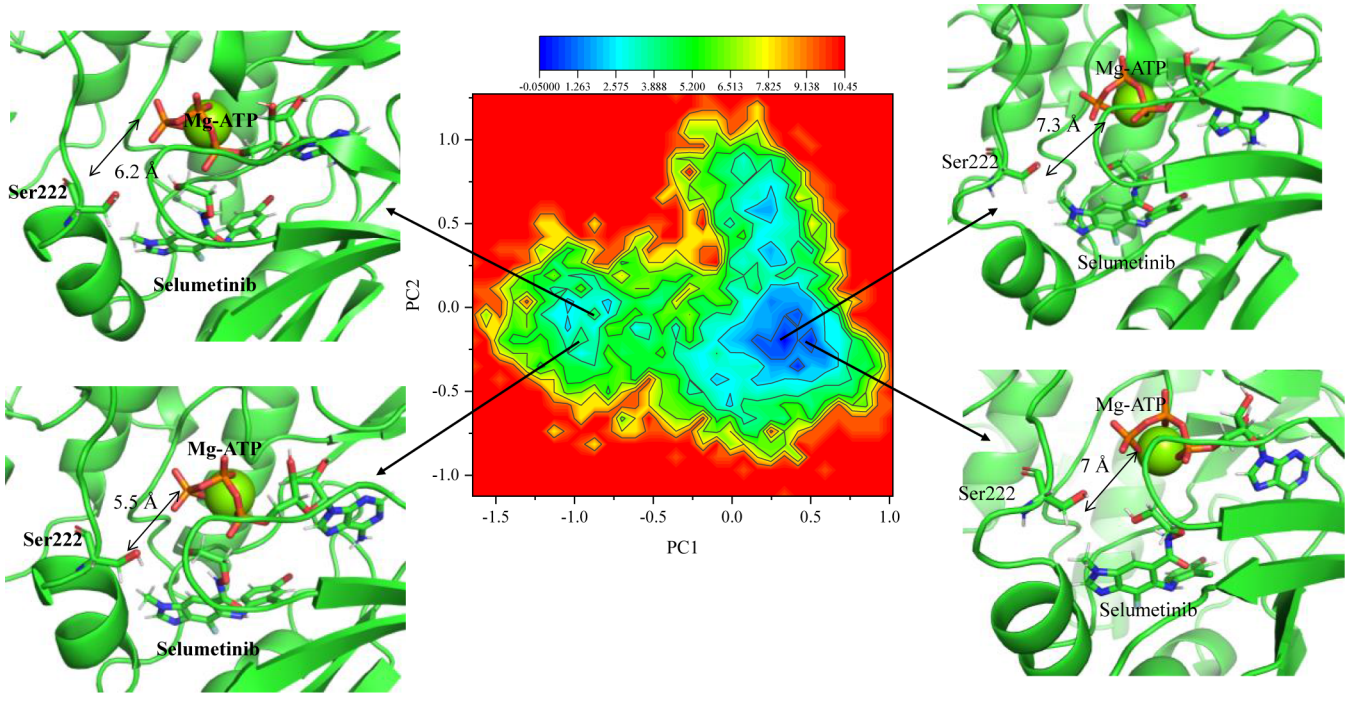

Figure 11. Free energy landscape of MEK1 with selumetinib. Free energy landscape is derived using the projection of principal component-1 (PC1) and principal component-2 (PC2). Blue color represents low-energy regions, and red indicates high-energy regions.

conformational changes in the activation loop, inhibiting the activation of MEK1.

Essential Dynamics of MEK1. Principal component analysis (PCA) provides a detailed picture of biomolecular motions by reducing the dimensionality using the covariance matrix of all conformations. The first few principal components (PCs) describe the most important collective system modes related to the functional motions of a biomolecular system. The free energy surface (FES) constructed from PC1 and PC2 can provide insights into the dynamic processes that occur in MEK1 for apo and selumetinib. FES corresponding to apo reveals that the activation loop can come closer to ATP and those conformations fall in the relatively lower energy regions (Figure 10). However, it can be noted from Figure 11 that the same event does not occur in the presence of selumetinib and other allosteric inhibitors.

FES allows the identification of dominant conformational states such as the activation loop close to ATP with relatively

https://doi.org/10.1021/acsomega.4c03615
ACS Omega 2024, 9, 31946−31956

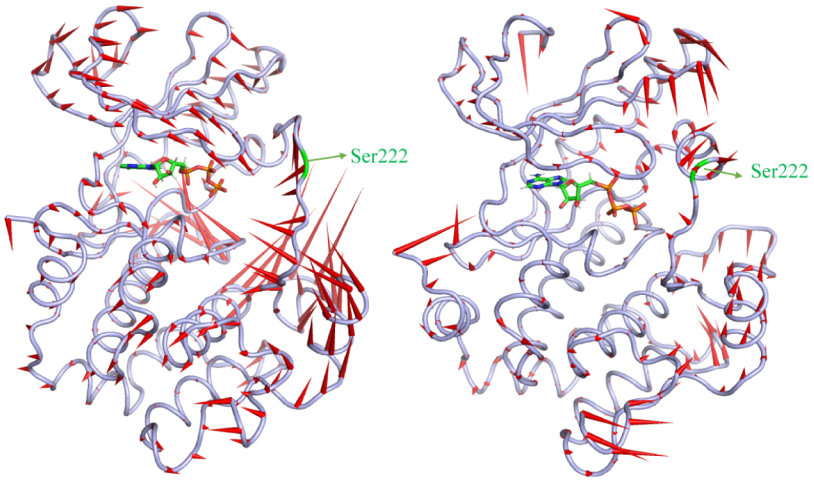

Figure 12. Projection of motion corresponds to eigen vector-1 of MEK1 in the cases of apo and selumetinib. The motion of C-alpha atoms is denoted by headed arrows. The arrows indicate the magnitude and direction of motion.

low energies throughout the simulation. The extreme projections for PC1 and PC2 during 100 ns of MD simulation are shown in Figure 12.

The arrows show the magnitude and direction of the motion of residues. The projection of eigenvectors and eigenvalues to MEK1 gives information about the collective or slow motions corresponding to the phosphorylation process. The Pro-rich loop shows a highly fluctuated region compared with other loops. Pro-rich loop and Ser222 are in correlated motion toward the ATP site, whereas the C-terminal is in anticorrelated motion with the Pro-rich loop and activation loop. The activation loop not much involved in the motion corresponds to eigenvector-1 except Ser222. It clearly shows that the Pro-rich loop is pushing Ser222 toward ATP in the apo state. Ser222 in the activation loop and Pro-rich loop displays a greater motion in the apo state. Interestingly, selumetinib and other allosteric inhibitors suppress the magnitude of motion of the Pro-rich loop and Ser222. On the other hand, they increase the magnitude of motion of the C-helix toward the activation loop. Previous study has analyzed the effect of active and nonactive mutations on dynamics and structure of MEK1 using molecular dynamics simulations.[58] The same study has shown that active mutations enhance the flexibility of activation and pro-rich loops, whereas the nonactive mutation reduced the dynamics of activation and Pro-rich loops when compared to wild types. The suppression of flexibility of the activation loop and Pro-rich loop by the allosteric inhibitors are correlated with the results of nonactive mutations. The suppression of the dynamics of the activation loop and Pro-rich loop reduces the accessibility of Ser222 to ATP.

CONCLUSIONS

Molecular dynamics simulations have been carried out to understand the structural changes that are necessary for the phosphorylation process of MEK1 in WT and in the presence of allosteric inhibitors. Various inhibitors such as selumetinib, cobimetinib, trametinib, pimasertib, and CH5126766 are considered for an understanding of the effect of allosteric inhibitors on the phosphorylation process. The MD simulations of WT MEK1 reveal that Ser222 moves toward ATP to transfer a proton to initiate the phosphorylation process. The same process, however, is not observed in the presence of allosteric inhibitors. The results show that a strong interaction of allosteric inhibitors with the activation loop restricts the movement of Ser222 toward Mg-ATP, which may be the dominant factor for the suppression of phosphorylation in MEK1/2. The allosteric inhibitors also restrict the structural changes in the activation loop, which facilitates the movement of Ser222 toward ATP. This research will provide novel insights to design effective anticancer therapeutics for targeting MEK1/2 in the future.

ASSOCIATED CONTENT

Supporting Information

The Supporting Information is available free of charge at https://pubs.acs.org/doi/10.1021/acsomega.4c03615.

Figure S1: comparison of root-mean-square deviation of MEK1 in the case of complexes of selumetinib, cobimetinib, trametinib, pimasertib, and CH5126766 with MEK1 for three independent simulations of 100 ns; Figure S2: calculated distance between ATP and Ser222 for wild type in the case of three independent simulations. (PDF)

AUTHOR INFORMATION

Corresponding Author

Sangwook Wu − *PharmCADD, 224, Engineering Building 7, Busan 48548, Korea; Department of Physics, Pukyong National University, Busan 48513, Korea;* orcid.org/0000-0001-5794-9477; Email: s.wu@pharmcadd.com

Authors

Sathish K. Mudedla − *PharmCADD, 224, Engineering Building 7, Busan 48548, Korea;* orcid.org/0000-0003-3173-5993

Hayoung Lee − *Drug Discovery Division, ISU Abxis, Seongnam-si, Gyeonggi-do 13488, Korea*

Jeom Ji Kim − *Drug Discovery Division, ISU Abxis, Seongnam-si, Gyeonggi-do 13488, Korea*

Seong Hun Jang − *PharmCADD, 224, Engineering Building 7, Busan 48548, Korea*

Munikumar R. Doddareddy − *PharmCADD, 224, Engineering Building 7, Busan 48548, Korea*

Swetha Y. Sanam − *PharmCADD, 224, Engineering Building 7, Busan 48548, Korea*

https://doi.org/10.1021/acsomega.4c03615
ACS Omega 2024, 9, 31946−31956

Rochish Gundabathula − *PharmCADD, 224, Engineering Building 7, Busan 48548, Korea*
Jang-June Park − *Drug Discovery Division, ISU Abxis, Seongnam-si, Gyeonggi-do 13488, Korea*

Complete contact information is available at: https://pubs.acs.org/10.1021/acsomega.4c03615

Notes

The authors declare no competing financial interest.

■ ACKNOWLEDGMENTS

This research has received funding support from the ISU Abxis (PRE2203 project) through the project collaboration with PharmCADD.

■ REFERENCES

(1) Keshet, Y.; Seger, R. The MAP kinase signaling cascades: A system of hundreds of components regulates a diverse array of physiological functions. *Methods Mol. Biol.* **2010**, *661*, 3−38.
(2) Sabio, G.; Davis, R. J. TNF and MAP kinase signaling pathways. *Semin. Immunol.* **2014**, *26*, 237−245.
(3) Plotnikov, A.; Zehorai, E.; Procaccia, S.; Seger, R. The MAPK cascades: Signaling components, nuclear roles and mechanisms of nuclear translocation. *Biochim. Biophys. Acta* **2011**, *1813*, 1619−1633.
(4) Rogers, D. F. The role of airway secretions in COPD: Pathophysiology, epidemiology and pharmacotherapeutic options. *COPD* **2005**, *2*, 341−353.
(5) Senawong, T.; Phuchareon, J.; Ohara, O.; Mccormick, F.; Rauen, K. A.; Tetsu, O. Germline mutations of MEK in cardio-facio-cutaneous syndrome are sensitive to MEK and RAF inhibition: implications for therapeutic options. *Hum. Mol. Genet.* **2007**, *17*, 419.
(6) Xie, J.; Ajibade, A. O.; Ye, F.; Kuhne, K.; Gao, S. J. Reactivation of Kaposi's sarcoma-associated herpesvirus from latency requires MEK/ERK, JNK and p38 multiple mitogen-activated protein kinase pathways. *Virology* **2008**, *371*, 139−154.
(7) Hsieh, H.-P.; Hsu, J.-T. Strategies of development of antiviral agents directed against influenza virus replication. *Curr. Pharm. Des.* **2007**, *13*, 3531−3542.
(8) Thompson, N.; Lyons, J. Recent progress in targeting the Raf/MEK/ERK pathway with inhibitors in cancer drug discovery. *Curr. Opin. Pharmacol.* **2005**, *5*, 350−356.
(9) Wortzel, I.; Seger, R. The ERK Cascade: Distinct Functions within Various Subcellular Organelles. *Genes & Cancer* **2011**, *2*, 195.
(10) Dudley, D. T.; Pang, L.; Decker, S. J.; Bridges, A. J.; Saltiel, A. R. A synthetic inhibitor of the mitogenactivated protein kinase cascade. *Proc. Natl. Acad. Sci. U. S. A.* **1995**, *92*, 7686−7689.
(11) Sebolt-Leopold, J. S.; et al. Blockade of the MAP kinase pathway suppresses growth of colon tumors in vivo. *Nature Med.* **1999**, *5*, 810−816.
(12) Frémin, C.; Meloche, S. From basic research to clinical development of MEK1/2 inhibitors for cancer therapy. *J. Hematol. Oncol.* **2010**, *3*, 8.
(13) Knighton, D. R.; Zheng, J. H.; Eyck, L. T.; Ashford, V. A.; Xuong, N. H.; Taylor, S. S.; Sowadski, J. M. Crystal structure of the catalytic subunit of cyclic adenosine monophosphate-dependent protein kinase. *Science* **1991**, *253*, 407−414.
(14) Taylor, S. S.; Kornev, A. P. Protein kinases: Evolution of dynamic regulatory proteins. *Trends Biochem. Sci.* **2011**, *36*, 65−77.
(15) Atefi, M.; Euw, E. V.; Attar, N.; Ng, C.; Chu, C.; Guo, D.; Nazarian, R.; Chmielowski, B.; Glaspy, J. A.; Comin-Anduix, B.; et al. Reversing Melanoma Cross-Resistance to BRAF and MEK Inhibitors by Co-Targeting the AKT/mTOR Pathway. *PLoS One* **2011**, *6*, No. e28973.
(16) Roskoski, R., Jr MEK1/2 dual-specificity protein kinases: Structure and regulation. *Biochem. Biophys. Res. Commun.* **2012**, *417*, 5−10.
(17) Kolch, W. Coordinating ERK/MAPK signalling through scaffolds and inhibitors. *Nat. Rev. Mol. Cell Biol.* **2005**, *6*, 827−837.
(18) Shi, H.; Kong, X.; Ribas, A.; Lo, R. S. Combinatorial treatments that overcome PDGFRÎ²-driven resistance of melanoma cells to V600EB-RAF inhibition. *Cancer Res.* **2011**, *71*, 5067−5074.
(19) Liu, B.; Fisher, M.; Groves, P.; et al. Down-regulation of the ERK1 and ERK2 mitogen-activated protein kinases using antisense oligonucleotides inhibits intimal hyperplasia in a porcine model of coronary balloon angioplasty. *Cardiovasc. Res.* **2002**, *54* (3), 640.
(20) Kamata, T.; et al. Dephosphorylation of MEK1 by protein phosphatase 2A and Cdc25A at centrosomes. *Cell Struct. Funct.* **2010**, *35*, 49−59.
(21) Bollag, G.; Hirth, P.; Tsai, J.; Zhang, J.; Ibrahim, P. N.; Cho, H.; et al. Clinical efficacy of a RAF inhibitor needs broad target blockade in BRAF-mutant melanoma. *Nature* **2010**, *467*, 596−599.
(22) Carlino, M. S.; Fung, C.; Shahheydari, H.; Todd, J. R.; Boyd, S. C.; Irvine, M.; et al. Preexisting MEK1P124 mutations diminish response to BRAF inhibitors in metastatic melanoma patients. *Clin. Cancer Res.* **2015**, *21*, 98.
(23) Shao, Y.; Aplin, A. E. Akt3-mediated resistance to apoptosis in B-RAF-targeted melanoma cells. *Cancer Res.* **2010**, *70*, 6670.
(24) Smalley, K. S. M.; Lioni, M.; Palma, M. D.; Xiao, M.; Desai, B.; Egyhazi, S.; et al. Increased cyclin D1 expression can mediate BRAF inhibitor resistance in BRAF V600E−mutated melanomas. *Mol. Cancer Ther.* **2008**, *7*, 2876.
(25) Xing, F.; Persaud, Y.; Pratilas, C. A.; Taylor, B. S.; Janakiraman, M.; She, Q. B. Concurrent loss of the PTEN and RB1 tumor suppressors attenuates RAF dependence in melanomas harboring V600EBRAF. *Oncogene* **2012**, *31*, 446.
(26) Ohren, J. F.; Chen, H.; Pavlovsky, A.; Whitehead, C.; Zhang, E.; Kuffa, P.; Yan, C.; McConnell, P.; Spessard, C.; Banotai, C.; et al. Charles A Hasemann. Structures of human MAP kinase kinase 1 (MEK1) and MEK2 describe novel noncompetitive kinase inhibition. *Nat. Struct. Mol. Biol.* **2005**, *12* (3), 278.
(27) Roskoski, R., Jr MEK1/2 dual-specificity protein kinases: Structure and regulation. *Biochem. Biophys. Res. Commun.* **2012**, *417*, 5−10.
(28) Haling, J. R.; Sudhamsu, J.; Yen, I.; Sideris, S.; Sandoval, W.; Phung, W.; Bravo, B. J.; Giannetti, A. M.; Peck, A.; Masselot, A. Crystal structure of the BRAF: MEK1 complex. *Cancer Cell* **2014**, *26*, 402−413.
(29) Caunt, C. J.; Caunt, M. J.; Sale, M. J.; Smith, P. D.; Cook, S. J. MEK1 and MEK2 inhibitors and cancer therapy: The long and winding road. *Nat. Rev. Cancer* **2015**, *15*, 577−592.
(30) Han, J.; Liu, Y.; Yang, S.; Wu, X.; Li, H.; Wang, Q. MEK inhibitors for the treatment of non-small cell lung cancer. *J. Hematol. Oncol.* **2021**, *14*, 1.
(31) Cheng, Y.; Tian, H. Current Development Status of MEK Inhibitors. *Molecules* **2017**, *22*, 1551.
(32) Wang, C.; Wang, H.; Zheng, C.; Liu, Z.; Gao, X.; Xu, F.; Niu, Y.; Zhang, L.; Xu, P. Research progress of MEK1/2 inhibitors and degraders in the treatment of cancer. *Eur. J. Med. Chem.* **2021**, *218*, 113386.
(33) Gonzalez-Del Pino, G. L.; Li, K.; Park, E.; Schmoker, A. M.; Ha, B. H.; Eck, M. J. Allosteric MEK inhibitors act on BRAF/MEK complexes to block MEK activation. *Proc. Natl. Acad. Sci. U. S. A.* **2021**, *7*, No. e2107207118.
(34) Barrett, S. D.; Bridges, A. J.; Dudley, D. T.; Saltiel, A. R.; Fergus, J. H.; Flamme, C. M.; et al. The discovery of the benzhydroxamate MEK inhibitors CI-1040 and PD 0325901. *Bioorg. Med. Chem. Lett.* **2008**, *18*, 6501−6504.
(35) Robarge, K. D.; Lee, W.; Eigenbrot, C.; Ultsch, M.; Wiesmann, C.; Heald, R.; Price, S.; Hewitt, J.; Jackson, P.; Savy, P.; et al. Structure based design of novel 6,5 heterobicyclic mitogen-activated protein kinase kinase (MEK) inhibitors leading to the discovery of imidazo[1,5-a] pyrazine G-479. *Bioorg. Med. Chem. Lett.* **2014**, *24*, 4714−4723.
(36) Jumper, J.; et al. Highly accurate protein structure prediction with AlphaFold. *Nature* **2021**, *596*, 583−589.

(37) Varadi, M.; et al. AlphaFold Protein Structure Database: massively expanding the structural coverage of protein-sequence space with high-accuracy models. *Nucleic Acids Res.* **2022**, *50*, D439−D444.
(38) Eberhardt, J.; Santos-Martins, D.; Tillack, A. F.; Forli, S. AutoDock Vina 1.2.0: New Docking Methods, Expanded Force Field, and Python Bindings. *J. Chem. Inf. Model.* **2021**, *61* (8), 3891−3898.
(39) Trott, O.; Olson, A. J. AutoDock Vina: improving the speed and accuracy of docking with a new scoring function, efficient optimization, and multithreading. *J. Comput. Chem.* **2010**, *31*, 455−461.
(40) Berendsen, H. J. C.; van der Spoel, D.; van Drunen, R. GROMACS: A message-passing parallel molecular dynamics implementation. *Comput. Phys. Commun.* **1995**, *91*, 43−56.
(41) Lindahl, E.; Hess, B.; Van Der Spoel, D. GROMACS 3.0: a package for molecular simulation and trajectory analysis. *Mol. Model. Ann.* **2001**, *7*, 306−317.
(42) Hess, B.; Kutzner, C.; Van Der Spoel, D.; Lindahl, E. GROMACS 4: algorithms for highly efficient, load-balanced, and scalable molecular simulation. *J. Chem. Theory Comput.* **2008**, *4*, 435−447.
(43) Lindorff-Larsen, K.; Piana, S.; Palmo, K.; Maragakis, P.; Klepeis, J. L.; Dror, R. O.; Shaw, D. E. Improved side-chain torsion potentials for the Amber ff99SB protein force field. Proteins. *Proteins: struct., Funct., Bioinf.* **2010**, *78*, 1950−1958.
(44) Li, P.; Roberts, B. P.; Chakravorty, D. K.; Merz, K. M. Rational Design of Particle Mesh Ewald Compatible Lennard-Jones Parameters for +2 Metal Cations in Explicit Solvent. *J. Chem. Theory Comput.* **2013**, *9*, 2733−2748.
(45) Frisch, M.; Trucks, G.; Schlegel, H.; Scuseria, G.; Robb, M.; Cheeseman, J.; Scalmani, G.; Barone, V.; Petersson, G.; Nakatsuji, H. *Gaussian 16 rev.*; Gaussian, Inc, 2016.
(46) Wang, J.; Wang, W.; Kollman, P. A.; Case, D. A. Automatic atom type and bond type perception in molecular mechanical calculations. *J. Mol. Graphics Modell.* **2006**, *25*, 247−260.
(47) Jorgensen, W. L.; Chandrasekhar, J.; Madura, J. D.; Impey, R. W.; Klein, M. L. Comparison of simple potential functions for simulating liquid water. *J. Chem. Phys.* **1983**, *79*, 926−935.
(48) Parrinello, M.; Rahman, A. Polymorphic transitions in single crystals: A new molecular dynamics method. *J. Appl. Phys.* **1981**, *52*, 7182−7190.
(49) Nosé, S.; Klein, M. L. Constant Pressure Molecular Dynamics for Molecular Systems. *Mol. Phys.* **1983**, *50*, 1055−1076.
(50) Bussi, G.; Donadio, D.; Parrinello, M. Canonical Sampling through Velocity Rescaling. *J. Chem. Phys.* **2007**, *126*, 014101.
(51) Darden, T.; York, D.; Pedersen, L. Particle mesh Ewald: An N.log (N) method for Ewald sums in large systems. *J. Chem. Phys.* **1993**, *98*, 10089−10092.
(52) Hess, B.; Bekker, H.; Berendsen, H. J.; Fraaije, J. G. LINCS: a linear constraint solver for molecular simulations. *J. Comput. Chem.* **1997**, *18*, 1463−1472.
(53) Zwanzig, R. W. High-Temperature Equation of State by a Perturbation Method. I. Nonpolar Gases. *J. Chem. Phys.* **1954**, *22*, 1420−1426.
(54) Mey, A.S. J. S.; Allen, B. K.; Macdonald, H. E.; Chodera, J. D.; Hahn, D. F.; Kuhn, M.; Michel, J.; Mobley, D. L.; Naden, L. N.; Prasad, S.; et al. Best Practices for Alchemical Free Energy Calculations. *Living J. Comput. Mol. Sci.* **2020**, *2*, 18378.
(55) DeLano, W. L. Pymol: An open-source molecular graphics tool CCP4 Newsl. *Protein Crystallogr.* **2002**, *40*, 82−92.
(56) Bennett, C. H. Efficient estimation of free energy differences from Monte Carlo data. *J. Comput. Phys.* **1976**, *22*, 245−268.
(57) Kubota, Y.; Fujioka, Y.; Patil, A.; Takagi, Y.; Matsubara, D.; Iijima, M.; Momose, I.; Naka, R.; Nakai, K.; Noda, N. N.; Takekawa, M. Qualitative differences in disease-associated MEK mutants reveal molecular signatures and aberrant signaling-crosstalk in cancer. *Nat. Commun.* **2022**, *13*, 2022.
(58) Liu, Y.; Zhu, J.; Guo, X.; Huang, T.; Han, J.; Gao, J.; Xu, D.; Han, W. How oncogenic mutations activate human MAP kinase 1 (MEK1): A molecular dynamics simulation study. *J. Biomol. Struct. Dyn.* **2020**, *38*, 3942−3958.

https://doi.org/10.1021/acsomega.4c03615
ACS Omega 2024, 9, 31946−31956